IOSR Journal of Applied Chemistry (IOSR-JAC)
e-ISSN: 2278-5736. Volume 18, Issue 1 Ser. 1 (January 2025), PP 21-39
www.iosrjournals.org

Understanding The Structural, Electronic Features And Solvatochromic Behaviour Of Coumarin Derivatives Using Experimental And DFT Theory

Vinayaka Chandrappa Barangi, Lokesh Anand Shastri, Jyoti Nagalik, Sanjeev R Inamdar, Anilkumar R Patil, Umesh B. Hunagund, Varsha V. Koppal, Ullas N. Shetti

Department Of Chemistry, Karnatak University, Dharwad-580003, Karnataka, India
Department Of Chemistry, Karnatak Lingayat Education Parappa Channappa Jabin Science College, Hubballi-580031, Karnataka, India
Department Of Physics, Karnatak University, Dharwad – 580003, Karnataka, India
Department Of Chemistry, BLDEA's S. B. Arts And K. C. P. Science College, Vijayapur – 586103, Karnataka, India
KRCES's GGD Arts BMP Com And SVS Sci College, Bailhongal-580031 Karnataka, India
Department Of Physics, K.L.E Technological University, Hubli- 580031, Karnataka, India
Department Of Chemistry, Shri K.H. Patil Government First Grade College, Hulkoti- 591102, Karnataka, India

Abstract
*The absorption and fluorescence spectra of **3a**, **3b**,**3c** and**3d**compounds ware recorded in various solvents of different dielectric constant. It is observed that, changing the surrounding medium of the solute induces bathochromic shift, which is attributed due to **π→π*** transition in the spectral levels for all four compounds. Theoretically and experimentally the ground and excited state dipole moments of **3a**, **3b**,**3c** and **3d** compounds ware determined both theoretically and experimentally. Furthermore, theoretical calculations such as density functional theory (DFT) were performed to get a better understanding of the intramolecular charge transfer property and electronic structures of **3a**, **3b**,**3c** and**3d**compounds. The molecular electrostatic potential analysis provides the visual image of the chemically active sites and comparable reaction of atoms. The natural bond orbital analysis was performed to understand the molecular interaction on the basis of stability of molecule arising from hyper-conjugative interaction and charge delocalization.*

Keywords: *Absorption; Fluorescence; Solvatochromism, DFT calculations; NBO analysis.*

Graphical Abstract:

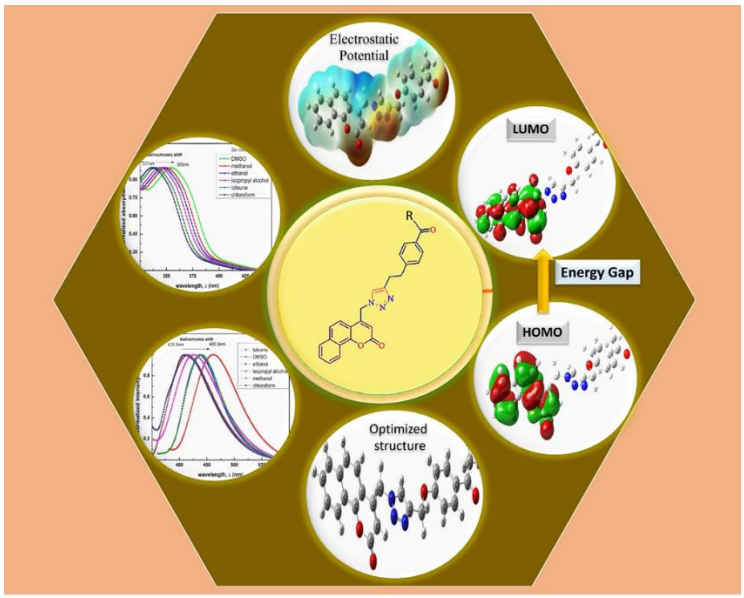

Date of Submission: 20-01-2025 Date of Acceptance: 30-01-2025

I. Introduction

Synthesis of heterocyclic compounds is most fascinating and advance area of research for various molecules of biologically and photophysical properties[1-2]from robust synthetic methods. Currently, heterocyclic chemistry offers powerful tools, which are efficiently applied for the preparation of new materials with defined physicochemical properties. Such as Organic light emitting diodes[OLEDs], laser Dyes, fluorescent materials for biochemical and biological imaging applications[3–6].

Coumarin and its analogues have got much importance in the creation of materials with specific photophysical properties such as OLED'S, as nonlinear optical chromospheres and sensors because of its enhanced emissive properties often exhibit strong luminescence[7].moreover, the coumarin derivatives of exhibits outstanding biocompatibility, high thermal stability, steady fluorescence emission and remarkable structural flexibility[8–10]. While Triazoles are important structural motif and synthesized high selectivity towards particular analytes of interest, via click chemistry and the generated 1,2,3-triazole-based chemosensors, have become an important structural motif in the field of chemical sensing[11]. To date, molecules have been generally exploited toward the fabrication and modification of several applications, such as drug, and corrosion inhibitor[12–14].However, the triazole molecule also have been widely used in molecular recognition, heterogeneous catalysis, bio-conjugation, pharmaceuticals[15].

Solvatochromism is one of the most useful method for comprehending the impact of solvent or charge distributions in both ground and excited states of the molecules. Because of its strong linear association between solvent polarity functions[16], The solvatochromic shifts approach is widely acknowledged among the available methods and is essential for evaluating the dipole moment of solute probes in their first electronically excited state. More recent the refinement of the classical theories ware successful via solvatochromic shift approach by extracting more important information about the electrostatic characteristics of a solute, orientation widening of absorption spectra, and electronic transitions[17]. Concern has grown over the mapping of molecular electrostatic potential (MESP) maps for chemical structure. Because it could provide important details on the interaction, active sites, and the process that determines whether a molecule will most likely undergo electrophilic or nucleophilic addition or substitution[18]. The concept of MESP holds great value in molecular modeling computations, since it can provide very accurate information about the active sites of several chemical entities along with the molecular surface[19].Although the theoretical calculation like DFT was performed for many compounds, a very useful theoretical calculation method for studying vibrational spectra and molecular structure. Numerous organic systems' vibrational spectra from DFT simulations show encouraging agreement with experimental findings[20].

Herein, our study supports the idea of solvatochromism and dipole moments of transient species. The Density functional theory (DFT) at basis set B3LYP/6-31 G (d,p)[21] will be used in theoretical calculations to examine ground state attributes such as molecular electrostatic potential maps (MEP), optimization structure, geometrical parameters, and reactivity parameters. Using DFT and the continuum polarizable salvation model PCM, the genesis of electronic spectra and the composition of the frontier molecular orbitals will be investigated. The natural atomic charge of each complex site will be determined using natural population analysis, and the inter- and intramolecular charge transfer within the created complex will be examined using natural bond order analysis (NBO).

II. Materials And Methods

Materials used

All the materials and reagents were analytical grade, obtained from commercial suppliers (Sigma Aldrich, S.D. Fine, Alfa Aesar, and Spectrochem), and used without additional purification. All melting points were determined using a Coslab Scientific melting point device and are unadjusted. Thin layer chromatography (TLC) was used to track the progress of reaction rates on precoated Merck silica gel $60F_{254}$ plates using an appropriate solvent system and spots were identified using UV light (λ = 254 nm). IR spectra were collected usinganhydrous potassium bromide (KBr) pellets on a Nicolet 170 SX FTIR spectrometer; the frequencies are reported in cm^{-1}. With a Bruker Avance FT NMR spectrometer (^1H NMR, 400 MHz and ^{13}C NMR, 100 MHz) spectra were collected using TMS as an internal standard, using $CDCl_3$ and DMSO-d_6 as a solvent. Shimadzu GCMSQP2010S and ESI/APCI-hybrid quadrupole, time-of-flight, and LC-MS mass spectrometers were used to record mass spectra (Synapt G2 HDMS ACQUITY UPLC).The emission spectra of the molecules ware obtained by the (Model: Hitachi F-7000, Japan) fluorescence spectrophotometer. The absorption spectra were obtained by UV-Visible spectrometer (Model: Hitachi U-3310, Japan).

General synthetic procedure

Synthesis of 1,2,3-triazolyl-methyl-2H-chromen-2-ones)[22]

To a solution of compounds (**1a**, **b**) (0.1 mol) in THF/H_2O, 1:1 (v:v), $CuSO_4 \cdot 5H_2O$ (0.015 mol), and sodium ascorbate (0.03 mol) were added. The reaction mixture was stirred at room temperature for half an hour

and subsequently 4-(azidomethyl)-2*H*-chromen-2-ones (**2a-d**) (0.1 mol) were added. The consequential reaction mixture was stirred for one hour at RT, and the completion of the reaction was monitored by TLC. The reaction mixture was then poured into ice cold water. The separated solid was filtered, washed with water and recrystallized from ethyl acetate to obtain the desired product (Fig 1: **3a**,**3b**,**3c** and**3d**.)

4-([4-([4-acetylphenoxy]methyl)-1H-1,2,3-triazol-1-yl]methyl)-2H-benzo[h]chromen-2-one

solid (Yield: 88%); m.p.: 118-120°C;**IR (KBr, cm^{-1})**: 1731 (Coumarin,C=O), 1655 (Ketone, C=O);**^{1}H NMR** (400 MHz, DMSO) δ (ppm): 2.48 (s, 3H, C(O)CH_3), 5.29(s, 2H, coumarin-C_4-CH_2), 5.95 (s, 1H, coumarin-C_3-H), 6.09 (s, 2H, O-CH_2), 7.13 (d, 2H, *J* = 8.8 Hz, ArH),7.72-7.75 (m, 2H, ArH), 7.82-7.92 (m, 4H, Ar-H),8.03-8.06 (m, 1H, ArH), 8.36-8.39 (m, 1H, ArH), 8.43 (s, 1H, ArH); **^{13}C NMR** (100 MHz, DMSO) δ (ppm): 26.4, 49.6, 61.2, 112.8, 113.4, 114.6, 120.3, 121.7, 122.2, 124.3, 125.9, 127.7, 128.0, 129.1, 130.2, 130.4, 150.1, 150.8, 159.3, 161.7, 189.4, 196.3; **MS** m/z: 426.

1-([4-([4-acetylphenoxy]methyl)-1H-1,2,3-triazol-1-yl]methyl)-3H-benzo[f]chromen-3-one

solid (Yield: 92%); m.p.: 130-132°C;**IR (KBr, cm^{-1})**: 1735 (Coumarin,C=O), 1668 (Ketone, C=O);**^{1}H NMR** (400 MHz, DMSO) δ (ppm): 2.49 (s, 3H, C(O)CH_3), 5.29(s, 2H, coumarin-C_4-CH_2), 5.47 (s, 1H, coumarin-C_3-H), 6.46 (s, 2H, O-CH_2), 7.11 (d, 2H, *J* = 8.4 Hz, ArH),7.58-7.69 (m, 3H, ArH), 7.87 (d, 2H, *J* = 8.4 Hz, Ar-H),8.09 (d, 1H,*J* = 8.0 Hz, ArH), 8.25 (d, 1H, *J* = 8.8 Hz, ArH), 8.37 (s, 1H, ArH), 8.43 (d, 1H, *J* = 8.4 Hz, Ar-H); **^{13}C NMR** (100 MHz, DMSO) δ (ppm): 26.5, 53.3, 61.3, 112.5, 113.0, 114.7, 117.5, 125.9, 128.6, 129.8, 130.5, 134.7, 143.0, 152.7, 154.4, 159.1, 161.8, 196.5; **MS** m/z: 425.

4-([1-([2-oxo-2H-benzo[h]chromen-4-yl]methyl)-1H-1,2,3-triazol-4-yl]methoxy)benzaldehyde

solid (Yield: 92%); m.p.: 136-138°C;**IR (KBr, cm^{-1})**: 1723 (Coumarin,C=O), 1670 (Aldehyde, C=O);**^{1}H NMR** (400 MHz, DMSO) δ (ppm): 5.33(s, 2H, coumarin-C_4-CH_2), 5.98 (s, 1H, coumarin-C_3-H), 6.11 (s, 2H, O-CH_2), 7.24 (d, 2H, *J* = 8.8 Hz, ArH),7.72-7.78 (m, 2H, ArH), 7.83-7.91 (m, 4H, Ar-H),8.05-8.07 (dd, 1H, *J* = 2.0, 4.0, 5.2 and 7.2 Hz, ArH), 8.38-8.40 (dd, 1H,*J* = 2.8, 4.0, 5.2 and 5.6 Hz, ArH), 8.47 (s, 1H, CHO); **^{13}C NMR** (100 MHz, DMSO) δ (ppm): 49.7, 61.4, 112.8, 115.3, 120.3, 121.7, 124.4, 126.1, 127.8, 128.1, 129.2, 130.0, 131.8, 134.5, 149.3, 150.9, 158.9, 158.4, 162.9, 175.7, 183.7, 191.5; **MS** m/z: 412.

4-([1-([3-oxo-3H-benzo[f]chromen-1-yl]methyl)-1H-1,2,3-triazol-4-yl]methoxy)benzaldehyde

solid (Yield: 89%); m.p.: 128-130°C;**IR (KBr, cm^{-1})**: 1736 (Coumarin,C=O), 1687 (Aldehyde, C=O);**^{1}H NMR** (400 MHz, DMSO) δ (ppm): 5.35(s, 2H, coumarin-C_4-CH_2), 5.51 (s, 1H, coumarin-C_3-H), 6.49 (s, 2H, O-CH_2), 7.23 (d, 2H, *J* = 8.8 Hz, ArH),7.62-7.72 (m, 3H, ArH), 7.85-7.88 (m, 2H, Ar-H),8.10-8.13 (dd, 1H,*J* = 1.0, 1.2, 6.8 and 8.0 Hz, ArH), 8.28 (d, 1H, *J* = 9.2 Hz, ArH), 8.40 (s, 1H, CHO), 8.45 (d, 1H, *J* = 8.8 Hz, Ar-H); **^{13}C NMR** (100 MHz, DMSO) δ (ppm): 53.1, 61.4, 112.4, 112.9, 115.2, 117.4, 125.4, 125.8, 126.1, 128.5, 129.7, 131.7, 134.5, 152.6, 154.3, 158.9, 162.8, 170.3, 191.3; **MS** m/z: 412.

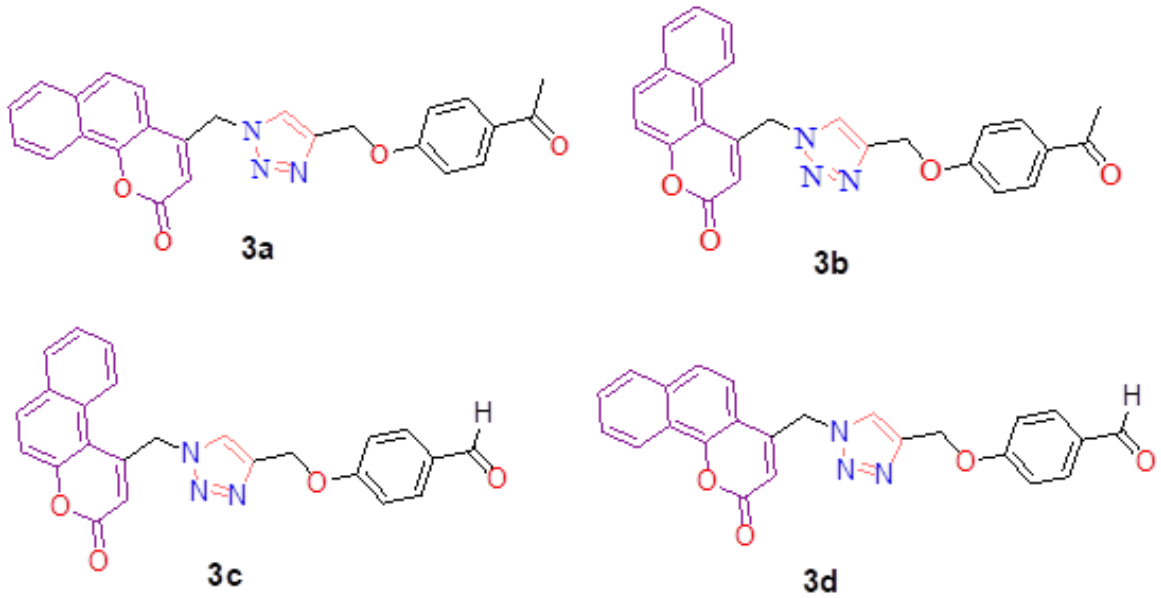

Fig.1. Chemical structures of synthesized compounds **3a,3b,3c** and **3d**

Computational Methods

In order to highlight the degree of molecular planarization, geometrical characteristics, frontier energy level delocalization, electronic structures, and to support the structure property relationship analysis of the optically significant synthesised compounds,the Gaussian 09 software was used to compute density functional theory (DFT) and time-dependent DFT (TD-DFT) calculations employing the hybrid functional Becke3–Lee–Yang–Parr (B3LYP) in conjunction with the 6-311G basis set in gas phase.

Solvatochromic shift approaches

Bilot and Kawaski[23-24] provided the detailed data to calculate the experimental electric dipole moments of fluorophore in liquid medium which are specified below

$\bar{\nu}_a - \bar{\nu}_f = m^{(1)}F(\varepsilon, n) + constant$ (1)

$\bar{\nu}_a + \bar{\nu}_f = -m^{(2)}\phi(\varepsilon, n) + constant$ (2)

Where $\phi(n, \varepsilon) = [F(n, \varepsilon) + 2g(n)]$.

In general the angle among μ_g and μ_e are collinear, or else it is analysed by equation (3), as specified below

$$cos\phi = \frac{1}{2\mu_g\mu_e}\left[\left(\mu_g{}^2 + \mu_e{}^2\right) - \frac{m^{(1)}}{m^{(2)}}\left(\mu_e{}^2 - \mu_g{}^2\right)\right] \quad (3)$$

The equation (4) and (5) given below are used to determine the fluorophore dipole moments of ground and excited state along with the help of the radius of cavity (*a*) and slopes secured according to the linear plots of equation (1) and (2)

$$\mu_g = \left(\frac{1}{2}(m^{(2)} - m^{(1)})\right)\sqrt{\frac{hca^3}{2m^{(1)}}} \quad (4)$$

$$\mu_e = \left(\frac{1}{2}(m^{(2)} + m^{(1)})\right)\sqrt{\frac{hca^3}{2m^{(1)}}} \quad (5)$$

Using the following equations (6) and (7) as given below, the solvent polarity functions are determined

$$F(n,\varepsilon) = \left[\frac{(2n^2+1)}{(n^2+2)}\right]\left(\frac{\varepsilon-1}{\varepsilon+2} - \frac{n^2-1}{n^2+2}\right) \quad (6)$$

and $$g(n,\varepsilon) = \frac{3}{2}\left[\frac{n^4-1}{(n^2+2)^2}\right] \quad (7)$$

As proposed by Lippert-Mataga[25–28] the equation (8), (9) and (10) are used to evaluatethe ground and excited state dipole moments of the fluorophore.

$\bar{\nu}_a - \bar{\nu}_f = m_1F_1(n, \varepsilon) + constant$ (8)

$\bar{\nu}_a - \bar{\nu}_f = m_2F_2(n, \varepsilon) + constant$ (9)

$\frac{\bar{\nu}_a+\bar{\nu}_f}{2} = m_3F_3(n, \varepsilon) + constant$ (10)

The solvent polarity functions are evaluated by the given equations.

$$F_1(n, \varepsilon) = \left[\left(\frac{(\varepsilon-1)}{(2\varepsilon+1)}\right) - \left(\frac{(n^2-1)}{(2n^2+1)}\right)\right] \quad (11)$$

$$F_2(n, \varepsilon) = \left[\frac{(2n^2+1)}{(n^2+2)}\right]\left[\left(\frac{\varepsilon-1}{\varepsilon+2}\right) - \left(\frac{n^2-1}{n^2+2}\right)\right] \quad (12)$$

$$F_3(n, \varepsilon) = \left\{\frac{1}{2}\frac{(2n^2+1)}{(n^2+2)}\left[\frac{\varepsilon-1}{\varepsilon+2} - \frac{n^2-1}{n^2+2}\right] + \frac{3}{2}\left[\frac{n^4-1}{(n^2+2)^2}\right]\right\} \quad (13)$$

The legitimacy of equations (8)-(10) is proved through the various solvents along with several ε and *n*, and the wavenumbers average value considered as a function of solvent polarity function by designing the stokes' shift. From the linear fit of equations (8) – (10), the slopes m_1, m_2 and m_3 are obtained.The μ_g and μ_e are determined from equations (17) – (18) which are parallel to each other.

$$\mu_g = \frac{m_3-m_2}{2}\left(\frac{hca^3}{2m_2}\right)^{\frac{1}{2}} \quad (17)$$

$$\mu_e = \frac{m_3+m_2}{2}\left(\frac{hca^3}{2m_2}\right)^{\frac{1}{2}} \quad (18)$$

and $$\mu_e = \frac{m_2+m_3}{m_3-m_2}\mu_g \; ; m_3 > m_2 \quad (19)$$

Suppaman's expression (20) is utilized to establish the Onsager cavity radius

$$a = \left(\frac{3M}{4\pi\delta N}\right)^{1/3} \quad (20)$$

Where δ□□Mand Nsignifies the density of solute, molecular weight and Avogadro's number, respectively.

III. Results And Discussion

Solvent Effects on Photophysical Properties

The typical absorption and fluorescence spectra of **3a**, **3b**,**3c** and**3d**molecules were recorded in different solvents. The absorption and fluorescence spectra of **3a**, **3b**,**3c** and **3d**moleculeswere shownin **Fig.2**,**3**,**4**and**5** respectively. Bilot-Kawaski's, Lippert's, Bakshiev's and Kawski-Chamma-Viallet's polarity functions were calculated using equations (6), (7) (11) (12) and (13) in different solvents and obtained results are shown in **Table 1.** The solvatochromic data of the studied molecules in different solvents are shown in **Table 2**. From **Table 2**, it is observed that, all the four studied compounds have shown a trend shift, on increasing the solvent polarity the absorption and fluorescence maxima shifted to longer wavelength side the bathochromic shift, may be attributed due to $\pi \rightarrow \pi^*$ transition in the spectral levels. The large magnitude of Stokes shift indicates that excited state geometry could be different from that of the ground state, and it also indicative of intermolecular charge transfer (ICT) nature of the excited state. The general observation is that there is an increase in Stokes shift values with increasing solvent polarity indicating that there is an increase in the dipole moment of excitation. In such cases, the relaxed excited state will be energetically stabilized relative to the ground state and a significant red shift of fluorescence is observed.

Table 1. The values of **ε**, **n** polarity parameters f_1, f_2, f_3 and $\phi(\varepsilon, n)$of different solvents.

Sl.No.	Solvents	ε	n	$f_1(\varepsilon,n)$	$f_2(\varepsilon,n)$	$f_3(\varepsilon,n)$	$\emptyset(n,\varepsilon)$
1	DMSO	46.68	1.478	0.263	0.841	0.743	1.487
2	Methanol	32.7	1.328	0.308	0.855	0.651	1.301
3	Ethanol	24.6	1.361	0.288	0.813	0.652	1.304
4	Isopropyl alcohol	20.33	1.385	0.275	0.779	0.648	1.296
5	Toluene	2.38	1.496	0.013	0.029	0.349	0.699
6	Chloroform	1.01	1.444	-0.206	-0.331	0.134	0.269

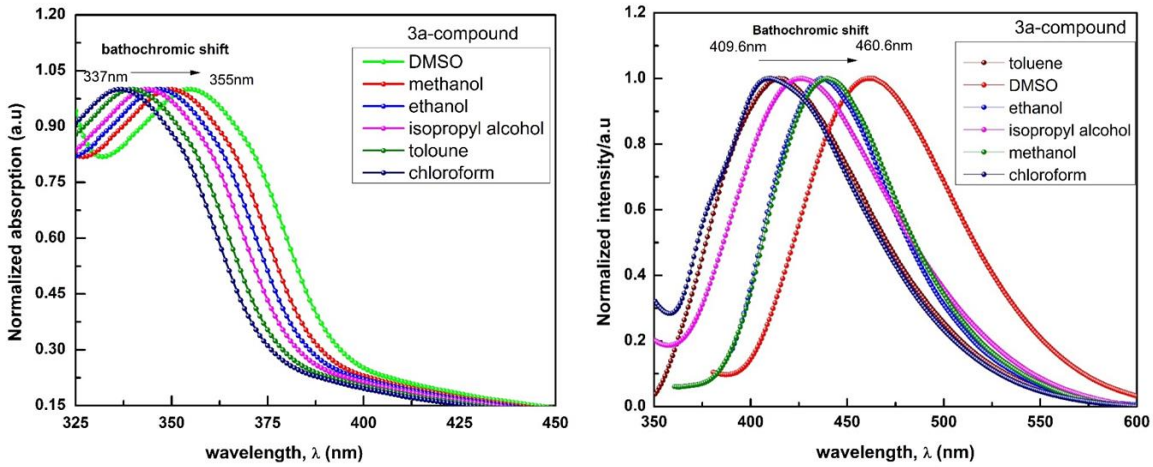

Fig.2. Absorption and fluorescence spectra of **3a** moleculein different solvents at room temperature**.**

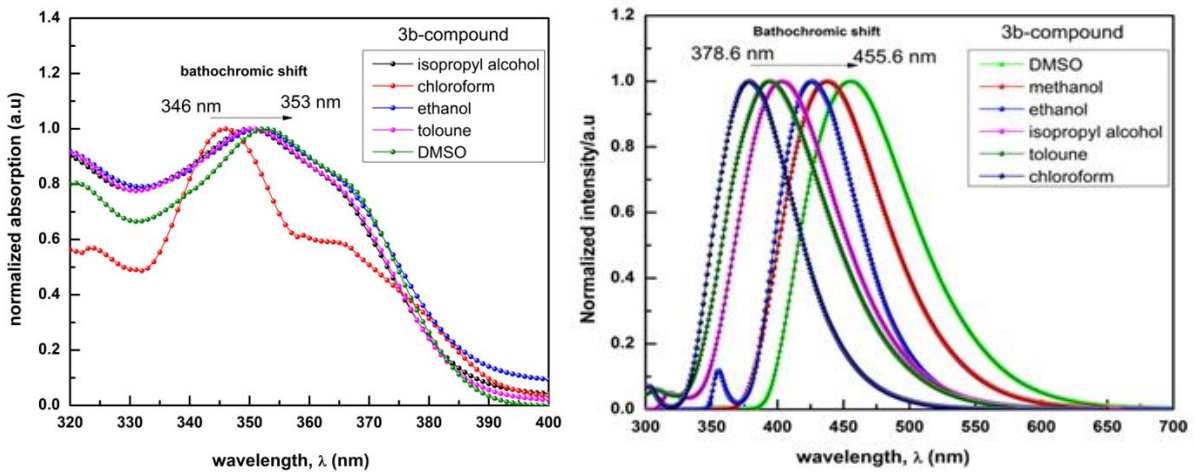

Fig.3. Absorption and fluorescence spectra of **3b** moleculein different solvents at room temperature

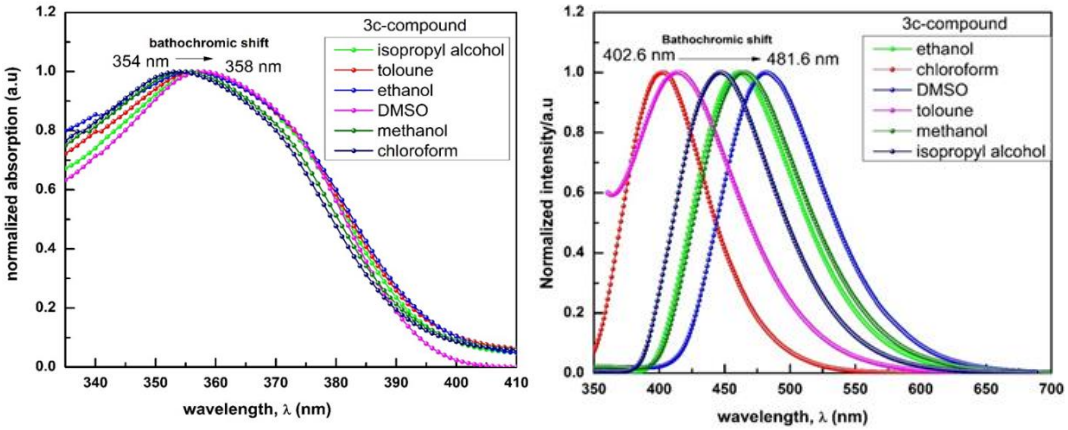

Fig.4. Absorption and fluorescence spectra of **3c**moleculein different solvents at room temperature

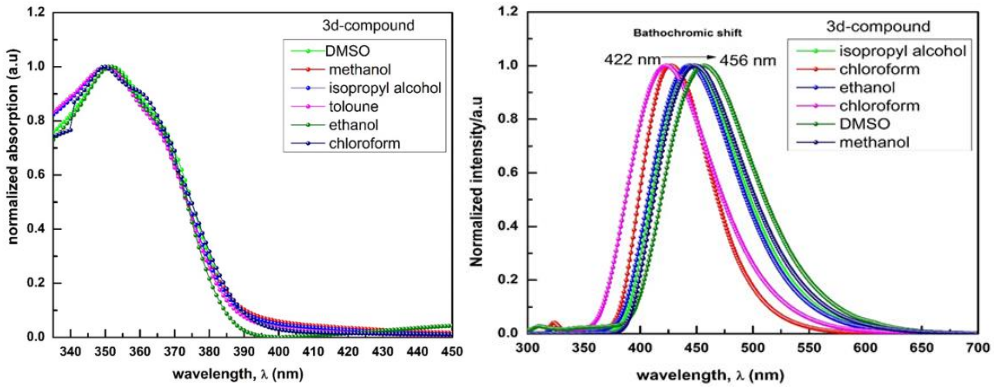

Fig.5. The Absorption spectra of **3d** moleculein different solvents at roomtemperature.

Table 2. Solvatochromic data of **3a**, **3b**,**3c** and **3d**Compounds in variousSolvents.

Solvents	λ_a **(nm)**	λ_f **(nm)**	$\bar{\nu}_a$ **(cm^{-1})**	$\bar{\nu}_f$ **(cm^{-1})**	$(\bar{\nu}_a - \bar{\nu}_f)$ **(cm^{-1})**	$(\bar{\nu}_a + \bar{\nu}_f)$ **(cm^{-1})**	$\frac{(\bar{\nu}_a + \bar{\nu}_f)}{2}$ **(cm^{-1})**
3a-Compound							
DMSO	355	450.6	28169.014	22192.632	5976.382	50361.646	25180.823
Methanol	350	439.6	28571.429	22747.953	5823.476	51319.381	25659.691
Ethanol	347	434.6	28818.444	23009.781	5808.378	51828.108	25914.054
Isopropyl Alcohol	344	426.0	29069.767	23474.178	5595.589	52543.946	26271.973
Toluene	340	414.6	29411.765	24119.633	5292.131	53531.398	26765.699
Chloroform	377	409.6	29673.591	24414.063	5259.528	54087.653	27043.827
3b-Compound							
DMSO	353	455.6	28328.612	21949.078	6379.534	50277.69	25138.845
Methanol	351	437.6	28490.028	22851.92	5638.109	51341.948	25670.974
Ethanol	351	425.6	28490.028	23496.241	4993.788	51986.269	25993.135
Isopropyl Alcohol	350	403.6	28571.429	24777.007	3794.422	53348.436	26674.218
Toluene	350	393.6	28571.429	25406.504	3164.925	53977.933	26988.966
Chloroform	346	378.6	28901.734	26413.101	2488.633	55314.835	27657.418
3c-Compound							
DMSO	358	481.6	27932.961	20764.12	7168.841	48697.08	24348.54
Methanol	357	465.6	28011.204	21477.663	6533.541	49488.868	24744.434
Ethanol	357	460.6	28011.204	21710.812	6300.392	49722.016	24861.008
Isopropyl Alcohol	357	446.6	28011.204	22391.402	5619.803	50402.606	25201.303
Toluene	356	413.6	28089.888	24177.95	3911.938	52267.837	26133.919
Chloroform	354	402.6	28248.588	24838.549	3410.038	53087.137	26543.568
3d-Compound							
DMSO	352	456.6	28409.091	21901.007	6508.083	50310.098	25155.049
Methanol	352	445.6	28409.091	22441.652	5967.439	50850.743	25425.371
Ethanol	352	448.6	28409.091	22291.574	6117.517	50700.665	25350.332
Isopropyl Alcohol	350	443.6	28571.429	22542.831	6028.597	51114.26	25557.13
Toluene	350	427.6	28571.429	23386.342	5185.086	51957.771	25978.885
Chloroform	350	422.6	28571.429	23663.038	4908.39	52234.467	26117.233

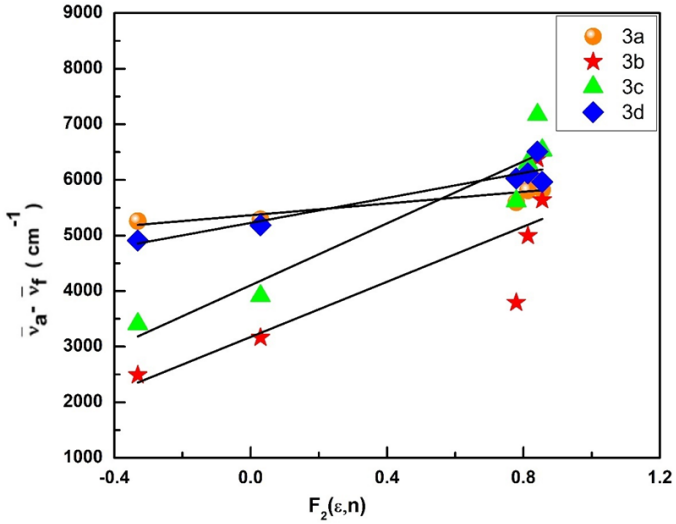

Fig.6. The Stoke's shift as a faction of $F_2(\varepsilon, n)$ for **3a**, **3b**,**3c** and **3d**molecules.

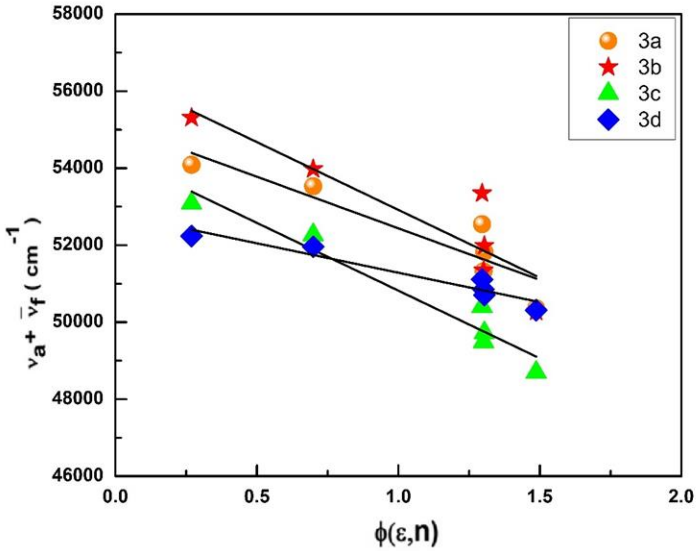

Fig.7. The Stoke's shift as a function of **ϕ(ε, n)** for **3a**, **3b**,**3c** and **3d**molecules.

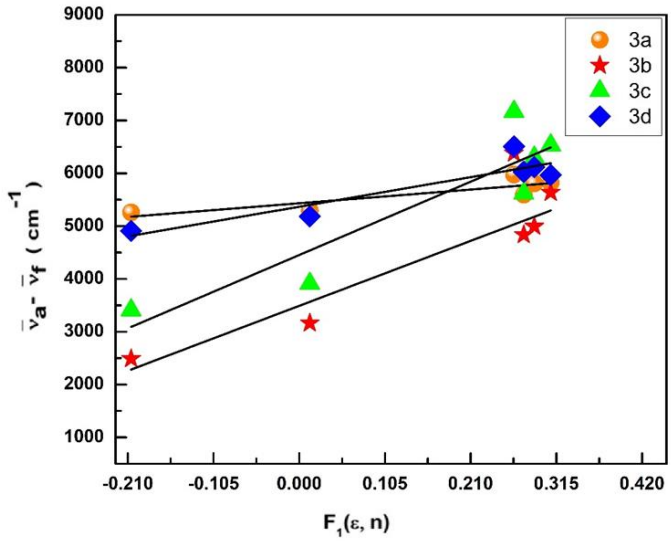

Fig. 8. Lippert's plot for **3a**, **3b**,**3c** and **3d**molecules.

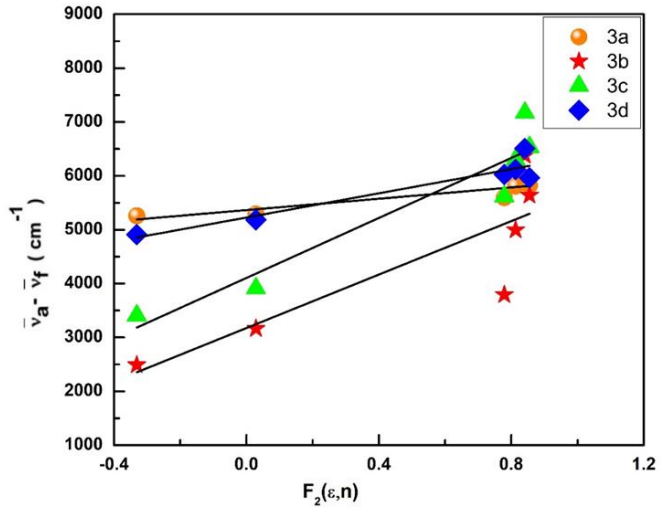

Fig.9. Bakshiev's plot for **3a**, **3b**,**3c** and **3d**molecules.

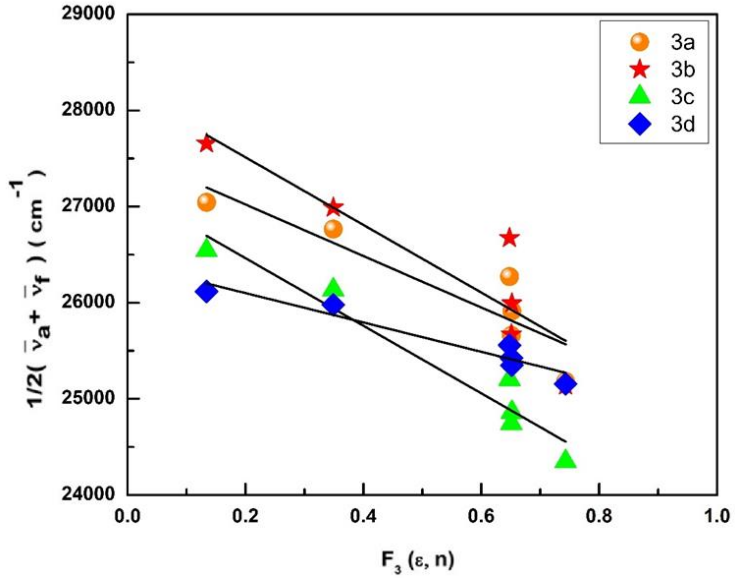

Fig.10. Kawski-Chamma-Viallet's plot for **3a**, **3b**,**3c** and **3d**molecules.

Further the electronic property of the molecule is very important phenomenon and is very sensitive on the electronics structure of the molecule hence the experiments for performed, using Bilot-Kawaski's equation (4) and (5) and estimated the dipole moment of all the four molecules in different solvents. A linear progression of $(\bar{\nu}_a - \bar{\nu}_f)$ versus f(ε,n) and $(\bar{\nu}_a + \bar{\nu}_f)$ versus $\phi(\varepsilon, n)$ have been plotted, the resulted data is fitted to a straight lineusing Origin-9 software and are shown in **Fig.6** and **Fig.**7while**Fig.8**, **8** and **9** correspond to Lippert's, Bakshiev's and Kawski-Chamma-Viallet's plots respectively.

Table 3. Different correlations, slopes (**m**), correlation factors (**r**) and number of solvents for all synthesized compounds

Correlations	Compound	Slope (m)	Correlation factor (r)	Number of solvents
BilotKawaski's	**3a**	2680.927	0.91	6
	3b	3519.456	0.80	
	3c	3517.783	0.92	
	3d	1527.535	0.90	
Lippert's	**3a**	1232.139	0.90	6
	3b	5857.733	0.80	
	3c	6613.512	0.80	
	3d	2670.153	0.80	
Bakhshiev's	**3a**	526.091	0.91	6
	3b	2481.541	0.84	

	3c	2784.349	0.90	
	3d	1123.208	0.90	
Kawski-Chamma-Viallet's	**3a**	2677.642	0.90	6
	3b	3515.874	0.80	
	3c	3514.678	0.93	
	3d	1526.017	0.90	

Table 4. Ground state and excited state dipole moments of **3a**, **3b**,**3c** and **3d**compounds.

Compound	**Radius** (Å)	$\mu_g^{\,a}$ $(\boldsymbol{D})$	$\mu_g^{\,b}$ $(\boldsymbol{D})$	$\mu_g^{\,c}$ (D)	$\mu_e^{\,d}$ (D)	$\mu_e^{\,e}$ $(\boldsymbol{D})$	$\mu_e^{\,f}$ $(\boldsymbol{D})$	$\mu_e^{\,g}$ $(\boldsymbol{D})$	$\mu_e^{\,h}$ $(\boldsymbol{D})$	$\mu_e^{\,i}$ $(\boldsymbol{D})$	ϕ^j
3a	3.402	2.94	2.93	9.289	13.71	4.36	4.37	5.13	4.37	6.17	0
3b	3.422	0.66	0.66	10.10	12.09	3.80	3.80	5.48	3.80	4.40	0
3c	3.450	0.44	0.44	9.404	14.01	3.81	3.81	5.64	3.81	4.23	0
3d	3.450	0.38	0.38	9.896	11.75	2.53	2.52	3.68	2.52	3.00	0

1 Debye (D) = 3.33564X10^{-30} cm = 10^{-18} esu cm,
[a] The ground state dipole moment calculated from Bilot-Kawaski Eqn.(1),
[b]The ground state dipole moment calculated using Eqn.17,
[c] The ground state dipole moment calculated using DFT/B2LYP/6-31G+(d,p),
[d] The excited state dipole moment calculated using DFT/B2LYP/6-31G+(d,p),
[e]The excited state dipole moment calculated using Bilot-Kawaski Eqn.(2),
[f] The excited state dipole moment calculated using Eqn.18,
[g]The experimental excited state dipole moment calculated from Lippert's equation,
[h] The experimental excited state dipole moment calculated from Bakshiev equation,
[i] The experimental excited state dipole moments calculated from Kawaski-Chamma-Viallet equation,
[j] The angle between ground state dipole moment and excited state dipole moment.

The statistical correlations of these fitted lines are shown in **Table 3**. From **Table 4**, it is observed that good correlation values are obtained in all most all cases. Some points are deviated may be due to specific solute-solvent interactions. Using these slope values, we have estimated the ground and excited state dipole moments of studied molecules using solvatochromic shift method. **Table 4** includes the ground state dipole moments which are calculated using equations (4) and (17) and excited state dipole moment calculated using equations (5), (8), (9), (10) and (19) respectively. The **Table 4** also includes the ground state and excited state dipole moment values computed from DFT B3LYP/6-31G+(d,p). From the **Table 4**, it is observed that experimental and theoretical ground state dipole moment values for **3a**, **3b**,**3c** and **3d**molecules differed, this discrepancy is like to arise upon of considering gas phase and ignoring the specific solvent-solute interactions for the theoretical calculation's[29–32].Also, the values of excited state dipole moment are greater than the ground state dipole moment. From these observations we conclude that the excited states of the present molecule are more polar than the corresponding ground state. However, the values of $\mu_e$obtained from different models are different owing to different assumptions made in the respective models. It is also observed that, the increase in dipole moments in the excited states is attributed to specific solvent effects such as hydrogen bonding, complex formation, etc.

HOMO-LUMO Study

Due to the absence of imaginary frequencies, the optimised geometries of every structure was verified as stable[33]. The lowest unoccupied molecular orbital (LUMO) and the highest occupied molecular orbital (HOMO) have different functions within the molecule. The HOMO is the highest energy level at which electrons acting as electron donors are occupied. On the other hand, an orbital with the lowest energy that can take electrons and function as an electron acceptor is known as the low-energy molecular orbital (LUMO)[34]. When combined, these so-called Frontier Molecular Orbitals (FMOs) offer a plausible qualitative estimate of both electron transport capacity and excitation properties. Furthermore, the reactivity of the molecules can be ascertained using these quantum chemical parameters. One of the key factors in understanding the various chemical properties of molecules, especially in the context of electronic transitions and reactivity is the band gap energy ((ΔE), which is computed from the corresponding HOMO and LUMO energy levels ($(\Delta E$ = E_{LUMO}-E_{HOMO}). The chemical properties such as HOMO-LUMO energy band gap (ΔE), chemical hardness (η), softness(δ),chemical potential (μ), optical bandgap energies(E_g) and electro negativity (χ) values are obtained from the HOMO and LUMO energies. Chemical hardness (η), and softness (δ)provides important information about photoelectric behaviour and charge transfer resistance of the compounds and The Lewis acid ability of the compound is measured by its electronegativity (χ)[35]. The theoretically designed E_{HOMO} and E_{LUMO} levels of the electronic structures **3(a-d)**are displayed in **Fig. 12**, with **Table 5** providing the corresponding energy level value. The electron clouds of HOMO energy levels are primarily found on the coumarin nucleus.

The electron clouds of the HOMO and the LUMO energy levels predominantly spread across the coumarin region of the target compounds, indicating the effective electron-donating and electron-deficient nature

of the coumarin nucleus. The smaller band gap energy (ΔE), generally indicates higher reactivity, which is linked to processes like charge transfer(CT), bond formation, and breakage. They also suggest good electrical conductivity and the possibility of using them in electronic devices. The computationally derived energy gap, through HOMO and LUMO values, are alignsclosely with optical band gaps obtained from absorption thresholds, indicating that a strong agreement between the two methods. The low chemical hardness (η) indicates soft nature of the molecules. Further the obtained results indicate the molecules are soft due to the small values of η and HOMO-LUMO energy gaps. This suggests that the small amount of energy is needed to excite soft molecules and one more significant parameter that has a notable impact on the mesomorphic behaviour of liquid crystals and the types of mesophases they exhibit is the dipole moment. This effect is explained by considering the level of molecular packing in mesophases, interactions, such as π-π stacking and quadrupolar interactions[36]. The dipole moment value of the x, y, and z axes as well as the total value were calculated for each compound in the studied series and results obtained are shown in the **Table 6**. The calculated ground and excited state dipole moments showed that, ground state the dipole moment values are smaller compared to those of excited state,which signifies a change in the electron distribution and energy levels within the molecule.

Molecular Electrostatic Potential (MEP) Study

Fig.13 displays the optimized ground-state molecular structures and molecular electrostatic potential maps for all the compounds.

The resulting molecular electrostatic potential (MEP) maps display a spectrum of colors, spanning from red to dark blue, signifying the presence of extreme negative and positive sites, respectively, within the structure under examination. The overall map layout progresses through colors in the sequence of red, yellow, green, light blue, and dark blue, representing a transition from the most negative to the most positive regions. The intense red coloration is observed in regions containing C=O group of aldehyde, keto derivatives with fused coumarin carbonyl group, indicating negative electrostatic potential and identifying them as electrophilic sites. Conversely, areas outside of these regions appear blue corresponds to triazole and substituted benzo group suggesting a positive electrostatic potential and characterizing them as nucleophilic sites.The most basic indicator of a molecule electron density are its atomic charges, which are also highly helpful in predicting the characteristics and reactivity of chemical bonds[37].

Compounds	HOMO	LUMO
3a	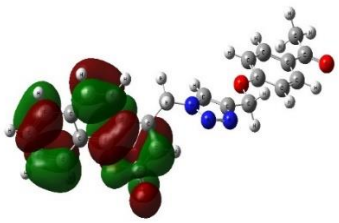	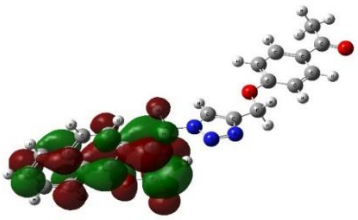
3b	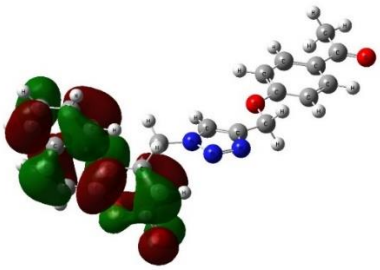	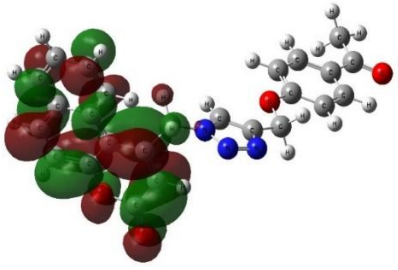
3c	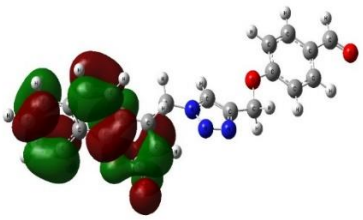	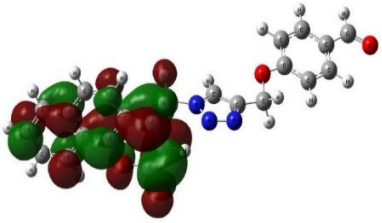

3d	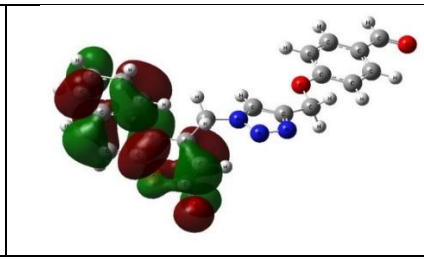	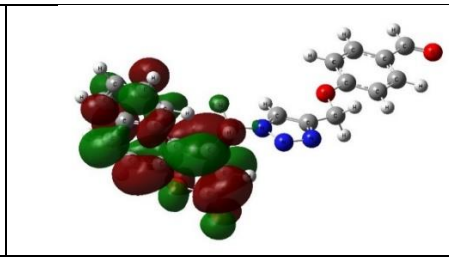

Fig.11.The Frontier Molecular Orbitals (HOMOs and LUMOs) diagrams of compound **3a**,**3b**,**3c** and **3d.**

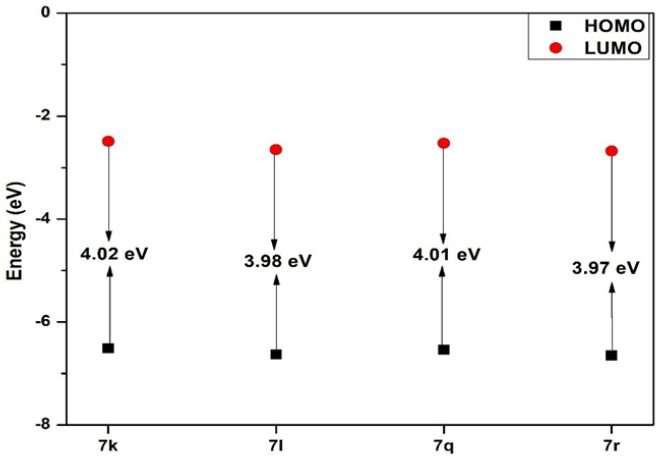

Fig.12. The HOMO-LUMO energy level diagram.

.

Compound	Geometry optimized structure	Molecular Electrostatic potential
3a	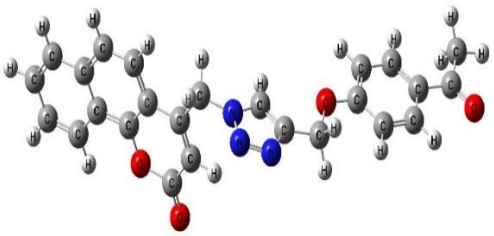	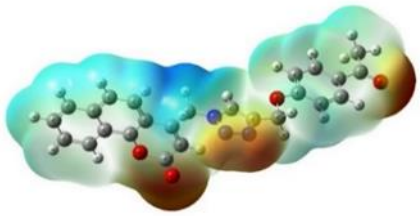
3b	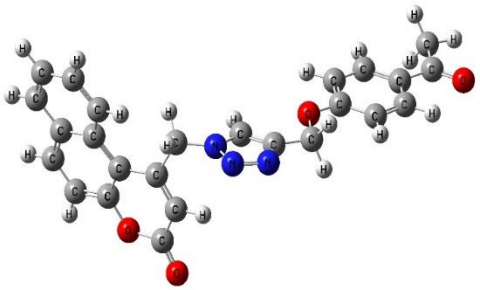	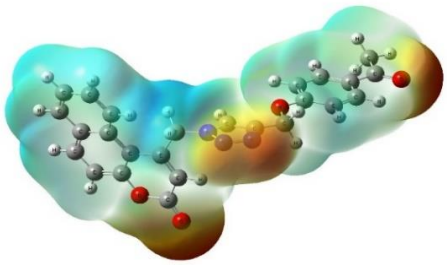
3c	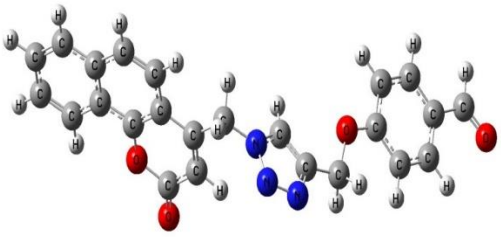	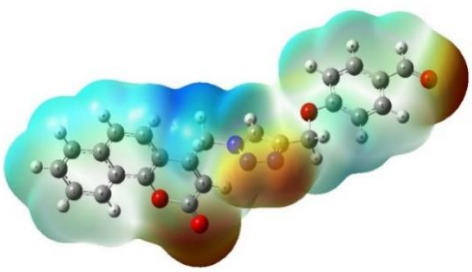

3d	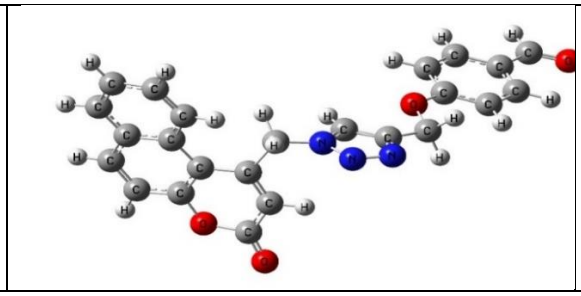	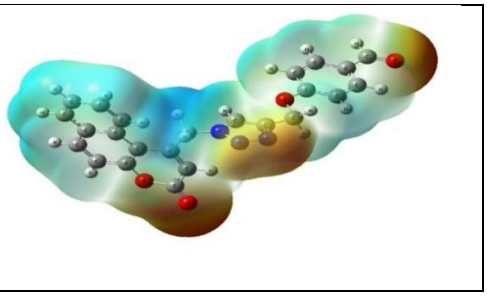

Fig.13. The optimized structure and molecular electrostatic potential (MESP) map of compounds

Table 5. HOMO, LUMO energies, energy band gap and some quantum chemical parameters for compound **3a, 3b, 3c,** and **3d** computed using DFT method employing Gaussian 09.

Compound	HOMO (eV)	LUMO (eV)	ΔE (eV)	E_g (eV)	η (eV)	δ (eV^{-1})	μ (eV)	χ (eV)
3a	-6.51250	-2.49202	4.02048	3.5782	2.01024	0.49745	4.50226	-4.50226
3b	-6.62706	-2.65011	3.97695	3.6258	1.98848	0.5029	4.63859	-4.63859
3c	-6.54135	-2.52766	4.01369	3.5714	2.00685	0.49829	4.53451	-4.53451
3d	-6.64883	-2.67841	3.97042	3.5879	1.98521	0.50373	4.66362	-4.66362

Table 6. Ground state and excited state dipole moment of all the compounds.

Molecule	μ_g	μ_e	$\Delta\mu$	λ_a
3a	9.2898	13.7154	4.4256	346.49
3b	10.0950	12.0962	2.0012	341.95
3c	9.4045	14.0112	4.6067	347.16
3d	9.8964	11.7583	1.8619	345.56

Mulliken Charge

Mulliken charges play a crucial role in comprehending molecular characteristics, reactivity, and interactions. These charges are derived through quantum mechanical approaches, particularly density functional theory (DFT). **Table 7** provides a breakdown of Mulliken charges assigned to individual atoms, aiding in the analysis of molecular properties and behaviour[38]. Adjacent C atom atomic charges increased while the net atomic charges of coordinating O and N atoms remained negative, suggesting that these atoms contributed electrons to coordinating atoms to improve electrostatic interactions.

Table 7. List of Mulliken Charges computed for **3a**, **3b**, **3c** and **3d** compounds using DFT method.

3a Molecule					
Sl. No.	**Atom**	**Charge (e)**	**Sl. No.**	**Atom**	**Charge (e)**
1	O	-0.34008	27	C	-0.09482
2	O	-0.5132	28	C	0.141576
3	N	-0.5517	29	C	-0.25663
4	N	0.032384	30	H	0.204312
5	N	-0.27453	31	C	0.490273
6	O	-0.54241	32	C	0.117025
7	C	-0.27085	33	C	0.224468
8	H	0.246447	34	H	0.225506
9	H	0.226614	35	C	0.0094
10	C	-0.12207	36	C	0.283689
11	H	0.213671	37	C	-0.19005
12	H	0.215562	38	H	0.170345
13	C	-0.18855	39	C	-0.07197
14	H	0.162293	40	H	0.165357
15	C	-0.11852	41	C	-0.12838
16	H	0.156837	42	C	-0.10035
17	C	-0.16652	43	H	0.187927
18	H	0.16031	44	C	-0.16139
19	C	-0.03095	45	H	0.184891
20	H	0.196321	46	C	0.311413
21	C	0.053204	47	C	-0.64553
22	C	-0.11706	48	H	0.205434
23	H	0.161206	49	H	0.204523
24	C	-0.10147	50	H	0.21269
25	H	0.162133	51	O	-0.36059
26	C	0.021805			

3b Molecule					
Sl. No.	**Atom**	**Charge (e)**	**Sl. No.**	**Atom**	**Charge (e)**
1	O	-0.45779	27	C	0.161135
2	O	-0.34652	28	C	0.17459
3	N	-0.52994	29	H	0.225082
4	N	0.063744	30	C	0.030972
5	N	-0.27781	31	C	0.268187
6	O	-0.51912	32	C	-0.18291
7	O	-0.35176	33	H	0.170065
8	C	-0.13316	34	C	-0.07376
9	H	0.157212	35	H	0.168287
10	C	-0.16271	36	C	-0.13343
11	H	0.165018	37	C	-0.08706
12	C	0.043061	38	H	0.18684
13	C	-0.1032	39	C	-0.16145
14	H	0.183118	40	H	0.189336
15	C	-0.16718	41	C	0.314191
16	H	0.154358	42	C	-0.30449
17	C	-0.05664	43	H	0.251318
18	C	-0.08264	44	H	0.221551
19	H	0.167713	45	C	-0.14639
20	C	-0.15353	46	H	0.210341
21	H	0.190384	47	H	0.213572
22	C	-0.07223	48	C	-0.64892
23	C	0.230024	49	H	0.202948
24	C	-0.24477	50	H	0.201633
25	H	0.208037	51	H	0.205641
26	C	0.439044			

3c molecule					
Sl. No.	**Atom**	**Charge (e)**	**Sl. No.**	**Atom**	**Charge (e)**
1	O	-0.34018	25	H	0.162327
2	O	-0.51289	26	C	0.022272
3	N	-0.54792	27	C	-0.09487
4	N	0.033032	28	C	0.139855
5	N	-0.27281	29	C	-0.25716
6	O	-0.53518	30	H	0.203154
7	C	-0.26969	31	C	0.490787
8	H	0.247161	32	C	0.117069
9	H	0.227227	33	C	0.219039
10	C	-0.13596	34	H	0.225496
11	H	0.215504	35	C	0.023182
12	H	0.214162	36	C	0.281094
13	C	-0.18871	37	C	-0.18742
14	H	0.162567	38	H	0.173536
15	C	-0.11823	39	C	-0.10845
16	H	0.157146	40	H	0.167483
17	C	-0.16656	41	C	-0.12888
18	H	0.160659	42	C	-0.06355
19	C	-0.03048	43	H	0.185518
20	H	0.196433	44	C	-0.17285
21	C	0.053391	45	H	0.187225
22	C	-0.11717	46	C	0.157919
23	H	0.161525	47	O	-0.36152
24	C	-0.10139	48	H	0.127107

3d molecule					
Sl. No.	**Atom**	**Charge (e)**	**Sl. No.**	**Atom**	**Charge (e)**
1	O	0.500941	25	H	0.205298
2	O	-0.34022	26	C	0.49242
3	N	-0.56187	27	C	0.165105
4	N	0.028925	28	C	0.237862
5	N	-0.27268	29	H	0.226063
6	O	-0.53879	30	C	0.004186
7	O	-0.36139	31	C	0.282951
8	C	-0.1289	32	C	-0.18726
9	H	0.159897	33	H	0.173886
10	C	-0.16509	34	C	-0.10925
11	H	0.165768	35	H	0.167497
12	C	0.057612	36	C	-0.12816

13	C	-0.11216	37	C	-0.06398
14	H	0.186567	38	H	0.185557
15	C	-0.16636	39	C	-0.17221
16	H	0.155817	40	H	0.187319
17	C	-0.05698	41	C	0.157866
18	C	-0.08968	42	C	-0.2705
19	H	0.169328	43	H	0.243134
20	C	-0.1507	44	H	0.242093
21	H	0.191325	45	C	-0.12603
22	C	-0.06572	46	H	0.214838
23	C	0.191691	47	H	0.216407
24	C	-0.26769	48	H	0.127136

NBO Analysis

Natural bond orbital (NBO) analysis is a powerful tool for studying molecular interactions and structures. The computations of natural bond orbitals (NBO) were conducted through the utilization of the NBO3.1program [39] that is incorporated in the Gaussian09 package, employing the density functional theory (DFT) method with B3LYP/6-311G basis set. For instance, studies have utilized NBO analysis to investigate electron delocalization in peptides and diagnose H-bonding interactions [40] and it has been employed to compare the interactions of molecules like Manzamines with antimalarials like Artemisinin and Quinine, providing insights into their stabilization energies and electron densities [41]. Another advantageous feature of the NBO method is its capability to provide insights into interactions occurring in both filled and virtual orbital spaces, thereby facilitating the examination of in traded intermolecular interactions. The utilization of the second-order fock matrix enables the assessment of donor-acceptor interactions within the framework of natural bond orbital analysis. By employing second order perturbation theory, the stabilization energy (E2) attributed to the delocalization from donor NBO (i) to acceptor NBO (j) can be quantified for all donor-acceptor pairs,

$$\text{E (2)} = \Delta E_{ij} = q_i \frac{(F_{ij})^2}{(E_j - E_i)}$$

where $F_{ij}$is the off-diagonal element of the NBO Fock matrix between orbitals i and j, $q_i$is the donor orbital occupancy, E_j&E_i are diagonal elements (orbital energies). **Table 8** summarizes the second-order perturbative estimates of donor-acceptor (bond-antibound) interactions in the NBO basis. The greater the E(2) value, the stronger the interaction between electron donor sand acceptors, leading to a higher propensity for electron donation from donors to acceptors and an increased level of conjugation within the entire system [42]. The interaction involving π* (C26 - C32) → π*(C21–C27), π* (C22 – C27) → π*(C12–C17), π* (C26 - C32) →π*(C21–C27), π* (C22 – C27) → π*(C12–C17) demonstrates the most substantial E (2) value of 264.79, 253.01, 259.53, 251.46 kcal/mol for **3a, 3b, 3c,** and **3d** molecules. The molecule exhibits significant interaction energy due to resonance, primarily involving electron donation from the lone pairs (LP (1)N3, LP (2) O2, LP (2) O6) to the antibonding acceptors (O1-C31, N4-N5, C36-C44). **Table 9** provides information on the electron occupancy and p-character in notable NBO natural atomic hybrid orbitals. A high percentage of p-character, nearly 100%, was observed in the π bonding orbitals as well as in the lone pair of nitrogen and oxygen.

Table 8. The second-order perturbation theory analysis of the Fock matrix in the NBO basis pertains to the intramolecular bonds of the compound **3a**, **3b**, **3c** and **3d**.

3a-Compound								
Donor(i)	**Type**	**ED/e**	**Acceptor(j)**	**Type**	**ED/e**	**E(2)**	**E(i)-E(j)**	**F(i,j)**
O1-C31	π	1.97798	O1-C31	π*	0.30178	1.03	0.36	0.018
			C28 -C29	π*	0.17864	6.44	0.39	0.047
N4-N 5	π	1.89251	C33 -C35	π*	0.32578	17.41	0.35	0.073
C13 -C15	π	1.72179	C17 -C19	π*	0.23879	16.98	0.29	0.064
			C21 -C27	π*	0.46944	18.46	0.28	0.067
C17 -C19	π	1.71494	C13 -C15	π*	0.25257	18.85	0.28	0.066
			C21 -C27	π*	0.46944	17.36	0.28	0.065
C21 -C27	π	1.55213	C13 -C15	π*	0.25257	15.74	0.28	0.062
			C17 -C19	π*	0.23879	16.91	0.28	0.065
			C22 -C24	π*	0.23536	15.61	0.27	0.061
			C26 -C32	π*	0.37550	22.8	0.26	0.07
C22 -C24	π	1.77975	C21 -C27	π*	0.46944	15.8	0.29	0.065
			C26 -C32	π*	0.37550	15.79	0.28	0.062
C26 -C32	π	1.65931	C21 -C27	π*	0.46944	14.23	0.3	0.06
			C22 -C24	π*	0.23536	16.66	0.3	0.065
			C26 -C32	π*	0.37550	1.37	0.29	0.018
			C28 -C29	π*	0.17864	17.8	0.3	0.068
C28 -C29	π	1.80533	O1-C31	π*	0.30178	25.95	0.28	0.078

			C7 -H 8	σ*	0.01523	2.84	0.66	0.04
			C7 -H 9	σ*	0.01671	2.4	0.65	0.037
			C26 -C32	π*	0.37550	11.21	0.3	0.054
C33 -C35	π	1.76617	N4-N 5	π*	0.47868	26.83	0.23	0.074
			C10 -H11	σ*	0.02425	2.46	0.66	0.038
			C10 -H12	σ*	0.02574	3.21	0.66	0.043
			C33 -C35	π*	0.32578	0.5	0.29	0.011
C36 -C44	π	1.64202	C36 -C44	π*	0.39418	0.95	0.28	0.015
			C37 -C39	π*	0.30332	16.19	0.29	0.062
			C41 -C42	π*	0.36895	24.1	0.3	0.076
C37 -C39	π	1.69930	C36 -C44	π*	0.39418	23.14	0.27	0.072
			C41 -C42	π*	0.36895	16.56	0.29	0.063
C41 -C42	π	1.62056	C36 -C44	π*	0.39418	18.23	0.26	0.061
			C37 -C39	π*	0.30332	23.26	0.27	0.072
			C41 -C42	π*	0.36895	0.83	0.28	0.014
			C46 -O51	π*	0.15583	22.03	0.25	0.07
C46 -O51	π	1.96870	C47 -H48	σ*	0.00657	1.93	0.74	0.034
			C47 -H49	σ*	0.00658	1.94	0.74	0.034
O2	n2	1.74032	O1-C31	π*	0.30178	32.89	0.32	0.092
			C26 -C32	π*	0.37550	30.47	0.34	0.094
N3	n1	1.53239	N4-N 5	π*	0.47868	39.74	0.23	0.086
			C33 -C35	π*	0.32578	33.1	0.3	0.092
O6	n2	1.84957	C36 -C44	π*	0.39418	27.92	0.33	0.091
O1-C31	π*	0.30178	C28 -C29	π*	0.17864	56.63	0.03	0.078
N4-N 5	π*	0.47868	C33 -C35	π*	0.32578	35.88	0.06	0.067
C21 -C27	π*	0.46944	C17 -C19	π*	0.23879	212.45	0.01	0.078
C26 -C32	π*	0.37550	C21 -C27	π*	0.46944	264.79	0.01	0.08
			C22 -C24	π*	0.23536	139.55	0.02	0.075
C36 -C44	π*	0.39418	C37 -C39	π*	0.30332	229.45	0.01	0.081
			C41 - C42	π*	0.36895	171.01	0.02	0.082
C46 -O51	π*	0.15583	C41 -C42	π*	0.36895	67.06	0.03	0.073

3b-Compound								
Donor(i)	**Type**	**ED/e**	**Acceptor(j)**	**Type**	**ED/e**	**E(2)**	**E(j)-E(j)**	**F(i,j)**
O2-C26	π	1.97752	O2-C26	π*	0.30297	1.04	0.36	0.019
			C23 -C24	π*	0.18091	6.62	0.39	0.047
N4-N 5	π	1.89301	C28 -C30	π*	0.32402	17.31	0.35	0.073
O7-C41	π	1.96871	C36 -C37	π*	0.36899	4.44	0.38	0.04
C8 -C10	π	1.71841	C12 -C17	π*	0.46366	17.69	0.28	0.066
			C13 -C15	π*	0.27473	19.83	0.28	0.067
C12 -C17	π	1.55340	C8 -C10	π*	0.25855	17.2	0.28	0.065
			C13 -C15	π*	0.27473	17.21	0.27	0.064
			C18 - C20	π*	0.22540	16.82	0.27	0.064
			C22 -C27	π*	0.37687	16.08	0.25	0.058
C13 -C15	π	1.72613	C8 -C10	π*	0.25855	17.15	0.29	0.063
			C12 -C17	π*	0.46366	17.49	0.28	0.066
C18 -C20	π	1.74387	C12 -C17	π*	0.46366	15.45	0.29	0.063
			C22 -C27	π*	0.37687	21.15	0.28	0.07
C22 -C27	π	1.66105	C12 -C17	π*	0.46366	16.48	0.3	0.064
			C18 -C20	π*	0.22540	13.88	0.3	0.06
			C22 -C27	π*	0.37687	1.41	0.28	0.018
			C23 -C24	π*	0.18091	17.24	0.3	0.067
C23 -C24	π	1.80466	O2-C26	π*	0.30297	25.63	0.28	0.077
			C22 -C27	π*	0.37687	10.69	0.29	0.052
C28 -C30	π	1.76351	N4-N 5	π*	0.48291	27.16	0.22	0.074
C31 -C39	π	1.64191	C31 -C39	π*	0.39409	0.95	0.28	0.015
			C32 -C34	π*	0.30327	16.19	0.29	0.062
			C36 -C37	π*	0.36899	24.11	0.3	0.076
C32 -C34	π	1.69946	C31 -C39	π*	0.39409	23.13	0.27	0.072
			C36 -C37	π*	0.36899	16.55	0.29	0.063
C36 -C37	π	1.62065	O7-C41	π*	0.15592	22.04	0.25	0.070
			C31 -C39	π*	0.39409	18.22	0.26	0.061
			C32 -C34	π*	0.30327	23.25	0.27	0.072
			C36 -C37	π*	0.36899	0.83	0.28	0.014
O1	n2	1.73516	O2-C26	π*	0.30297	33.44	0.32	0.093
			C22 -C27	π*	0.37687	30.96	0.33	0.093
N3	n1	1.53064	N4-N 5	π*	0.48291	39.76	0.23	0.086
O6	n2	1.84943	C31 -C39	π*	0.39409	27.95	0.33	0.091
N4-N 5	π*	0.48291	C28 -C30	π*	0.32402	35.18	0.06	0.067
O7-C41	π*	0.15592	C36 -C37	π*	0.36899	66.93	0.03	0.073
C22 -C27	π*	0.37687	C12 -C17	π*	0.46366	253.01	0.01	0.072
			C18 -C20	π*	0.22540	121.73	0.02	0.079
			C23 -C24	π*	0.18091	140.72	0.01	0.071
C31 -C39	π*	0.39409	C32 -C34	π*	0.30327	230.13	0.01	0.081
			C36 -C37	π*	0.36899	230.13	0.01	0.082

3c-Compound								
Donor(i)	**Type**	**ED/e**	**Acceptor(j)**	**Type**	**ED/e**	**E(2)**	**E(j)-E(j)**	**F(i,j)**
O1-C31	π	1.97796	O1-C31	π*	0.30201	1.03	0.36	0.018
			C28 -C29	π*	0.17936	6.45	0.39	0.047
N4-N 5	π	1.89163	C33 -C35	π*	0.32683	17.34	0.35	0.073
C13 -C15	π	1.72141	C17 -C19	π*	0.23859	16.97	0.29	0.064
			C21 -C27	π*	0.46949	18.48	0.28	0.067
C17 -C19	π	1.71471	C13 -C15	π*	0.25234	18.85	0.28	0.066
			C21 - C27	π*	0.46949	17.38	0.28	0.065
C21 -C27	π	1.55199	C13 -C15	π*	0.25234	15.72	0.28	0.062
			C17 -C19	π*	0.23859	16.89	0.28	0.065
			C22 -C24	π*	0.23512	15.61	0.27	0.061
			C26 -C32	π*	0.37585	22.84	0.26	0.07
C22 -C24	π	1.77975	C21 -C27	π*	0.46949	15.79	0.29	0.065
			C26 -C32	π*	0.37585	15.8	0.28	0.062
C26 -C32	π	1.65911	C21 -C27	π*	0.46949	14.21	0.3	0.06
			C22 -C24	π*	0.23512	16.63	0.3	0.065
			C28 -C29	π*	0.17936	17.87	0.3	0.068
C28 -C29	π	1.80564	C26 -C32	π*	0.37585	11.19	0.3	0.054
C33 -C35	π	1.76411	N4-N 5	π*	0.47772	26.93	0.23	0.074
C36 -C44	π	1.63354	C37 -C39	π*	0.29657	15.69	0.29	0.061
			C41 -C42	π*	0.37899	24.39	0.3	0.076
C37-C39	π	1.69556	C36 -C44	π*	0.39530	23.46	0.27	0.072
			C41 -C42	π*	0.37899	16.56	0.29	0.063
C41 -C42	π	1.61482	C36 -C44	π*	0.39530	18.15	0.26	0.061
			C37 -C39	π*	0.29657	22.82	0.27	0.072
			C46 -O47	π*	0.13208	22.49	0.25	0.071
O1	n2	1.82662	O2-C31	σ*	0.14277	41.93	0.49	0.129
O2	n2	1.74012	O1-C31	π*	0.30201	32.95	0.32	0.092
N3	n1	1.53027	N4-N 5	π*	0.47772	39.58	0.23	0.086
			C33 -C35	π*	0.32683	33.42	0.3	0.092
N4	n1	1.95583	N5-C35	σ*	0.03142	6.77	0.88	0.069
N5	n1	1.92797	N3-N 4	σ*	0.06242	9.79	0.67	0.073
O6	n2	1.84558	C36 -C44	π*	0.39530	28.45	0.33	0.092
O47	n2	1.89625	C46 -H48	σ*	0.05862	20.65	0.62	0.102
O1-C31	π*	0.30201	C28 -C29	π*	0.17936	57.32	0.03	0.078
C21 -C27	π*	0.46949	C17 -C19	π*	0.23859	210.32	0.01	0.078
C26 -C32	π*	0.37585	C21 -C27	π*	0.46949	259.53	0.01	0.08
	π*	0.37585	C22 -C24	π*	0.23512	137.28	0.02	0.075
C36 -C44	π*	0.39530	C37 -C39	π*	0.29657	195.82	0.01	0.081
	π*	0.39530	C41 -C42	π*	0.37899	177.14	0.02	0.082
C46 -O47	π*	0.13208	C41 -C42	π*	0.37899	57.12	0.03	0.074

3d-Compound								
3d-Compound								
Donor(i)	**Type**	**ED/e**	**Acceptor(j)**	**Type**	**ED/e**	**E(2)**	**E(j)-E(j)**	**F(i,j)**
O2-C26	π	1.97752	O2-C26	π*	0.30274	1.04	0.36	0.019
			C23 -C24	π*	0.18115	6.61	0.39	0.047
N4-N 5	π	1.89261	C28 -C30	π*	0.32472	17.3	0.35	0.073
O7-C41	π	1.97703	C36 -C37	π*	0.37891	5.03	0.39	0.043
C8 -C10	π	1.71834	C12 -C17	π*	0.46366	17.68	0.28	0.066
			C13 -C15	π*	1.72614	19.83	0.28	0.067
C12 -C17	π	1.55346	C8 -C10	π*	1.71834	17.19	0.28	0.065
			C13 -C15	π*	1.72614	17.21	0.27	0.064
			C18 -C20	π*	1.74378	16.83	0.27	0.064
			C22 -C27	π*	1.66067	16.1	0.25	0.058
C13 -C15	π	1.72614	C8 -C10	π*	1.71834	17.14	0.29	0.063
			C12 -C17	π*	0.46366	17.51	0.28	0.066
C18 -C20	π	1.74378	C12 -C17	π*	0.46366	15.44	0.29	0.063
C22 -C27	π	1.66067	C12 -C17	π*	0.46366	16.49	0.3	0.064
			C18 -C20	π*	1.74378	13.87	0.3	0.06
			C22 -C27	π*	1.66067	1.41	0.28	0.018
			C23 -C24	π*	0.18115	17.27	0.3	0.067
C23 -C24	π	1.80491	O2-C26	π*	0.30274	25.55	0.28	0.077
			C22 -C27	π*	1.66067	10.68	0.29	0.052
C28 -C30	π	1.76315	N4-N 5	π*	1.89261	27.18	0.22	0.074
C31 -C39	π	1.63368	C32 -C34	π*	1.55346	15.69	0.29	0.061
C32 -C34	π	1.69548	C31 -C39	π*	1.63368	23.47	0.27	0.072
			C36 - C37	π*	0.37891	16.56	0.29	0.063
C36 -C37	π	1.61478	O7-C41	π*	0.13196	22.48	0.25	0.071
			C31 -C39	π*	1.63368	18.16	0.26	0.061
			C32 -C34	π*	1.55346	22.83	0.27	0.072
O1	n2	1.73523	O2-C26	π*	0.30274	33.34	0.32	0.093
			C22 -C27	π*	1.66067	30.94	0.33	0.093
O2	n2	1.82840	O1-C26	σ*	0.14137	41.61	0.49	0.129
N3	n1	1.52939	N4-N 5	π*	1.89261	39.83	0.23	0.086
			C28 -C30	π*	0.32472	33.25	0.3	0.092
O6	n2	1.84581	C31 -C39	π*	1.63368	28.43	0.33	0.092
O2-C26	π*	0.30274	C23 -C24	σ*	0.18115	66.3	0.03	0.079
O7-C41	π*	0.13196	C36 -C37	π*	0.37891	57.13	0.03	0.074
C12 -C17	π*	0.46366	C8 -C10	π*	1.71834	234.01	0.01	0.079
C22 -C27	π*	0.37704	C12 -C17	π*	1.55346	251.46	0.01	0.072
	π*	0.37704	C18 -C20	π*	1.74378	122.17	0.02	0.079
	π*	0.37704	C23 -C24	π*	0.18115	144.98	0.01	0.071
C31 -C39	π*	0.39520	C32 -C34	π*	1.55346	195.43	0.01	0.081
	π*	0.39520	C36 -C37	π*	0.37891	176.9	0.02	0.082

Table 9. The NBO results indicate the presence of both Lewis and non-Lewis's orbitals in the **3a**, **3b**, **3c** and **3d**molecules.

3a-Compound						
Bond(A-B)	**ED/e**	**EDA%**	**EDB%**	**NBO**	**S%**	**P%**
πO1-C31	1.97798	67.41%	32.59%	0.8210 ($sp^{1.00}$)O1 0.5709 ($sp^{1.00}$)C 31	0.00%	100.00%
πN4-N 5	1.89251	50.87%	49.13%	0.7132($sp^{1.00}$)N4 0.7009($sp^{1.00}$) N5	0.00%	100.00%
πC13 -C15	1.72179	50.59%	49.41%	0.7113($sp^{1.00}$) C 13 0.7029($sp^{1.00}$) C 15	0.00%	100.00%
πC17 -C19	1.71494	50.94%	49.06%	0.7137($sp^{1.00}$)C 17 0.7005($sp^{1.00}$)C 19	0.00%	100.00%
πC21 -C27	1.55213	48.21%	51.79%	0.6943 ($sp^{1.00}$) C 21 0.7197($sp^{1.00}$) C 27	0.00%	100.00%
πC22 -C24	1.77975	49.48%	50.52%	0.7034($sp^{1.00}$)C 22 0.7108 ($sp^{1.00}$)C 24	0.00%	100.00%
πC26 -C32	1.65931	54.69%	45.31%	0.7395 ($sp^{1.00}$)C 26 0.6731 ($sp^{1.00}$)C 32	0.00%	100.00%
πC28 -C29	1.80533	46.57%	53.43%	0.6824 ($sp^{1.00}$)C 28 0.7309 ($sp^{1.00}$)C 29	0.00%	100.00%
πC33 -C 35	1.76617	48.97%	51.03%	0.6998($sp^{1.00}$)C33 0.7143($sp^{1.00}$)C 35	0.00%	100.00%
πC36 -C44	1.64202	46.26%	53.74%	0.6801($sp^{1.00}$)C 36 0.7331($sp^{1.00}$)C 44	0.00%	100.00%
πC37 -C39	1.69930	52.34%	47.66%	0.7234($sp^{1.00}$)C 37 0.6904($sp^{1.00}$)C 39	0.00%	100.00%
πC41 -C42	1.62056	55.68%	44.32%	0.7462 ($sp^{1.00}$)C 41 0.6657 ($sp^{1.00}$)C 42	0.00%	100.00%
πC46 -O 51	1.96870	33.70%	66.30%	0.5805($sp^{1.00}$)C 46 0.8143($sp^{1.00}$)C 51	0.00%	100.00%
n2O1	1.82651	-	-	$sp^{99.99}$	0.12%	99.88%
n2O2	1.74032	-	-	$sp^{1.00}$	0.00%	100.00%
n1N3	1.53239	-	-	$sp^{99.99}$	0.02%	99.98%
n1N4	1.95610	-	-	$sp^{0.95}$	51.17%	48.83%
n1N5	1.92798	-	-	$sp^{1.52}$	39.76%	60.24%
n2O6	1.84957	-	-	$sp^{1.00}$	0.01%	99.99%
n1O50	1.97683	-	-	$sp^{0.63}$	61.49%	38.51%
n2O51	1.90748	-	-	$sp^{99.99}$	0.02%	99.98%

3b-Compound						
Bond(A-B)	**ED/e**	**EDA%**	**EDB%**	**NBO**	**S%**	**P%**
πO2-C26	1.97752	67.38%	32.62%	0.8208($sp^{1.00}$)O2 0.5712($sp^{1.00}$)C26	0.01%	99.99%
πN4-N 5	1.89301	51.04%	48.96%	0.7144($sp^{1.00}$)N4 0.6997($sp^{1.00}$)N5	0.00%	100.00%
πO7-C41	1.96871	66.30%	33.70%	0.8143($sp^{1.00}$)O7 0.5805($sp^{1.00}$)C41	0.00%	100.00%
πC8-C10	1.71841	50.52%	49.48%	0.7108($sp^{1.00}$)C8 0.7034($sp^{1.00}$)C10	0.00%	100.00%
πC12-C17	1.55340	49.48%)	50.52%	0.7035($sp^{1.00}$)C12 0.7107($sp^{1.00}$)C17	0.00%	100.00%
πC13-C15	1.72613	51.31%	48.69%	0.7163($sp^{1.00}$)C13 0.6978($sp^{1.00}$)C15	0.00%	100.00%
πC18-C20	1.74387	48.24%	51.76%	0.6946($sp^{1.00}$)C18 0.7194($sp^{1.00}$)C20	0.00%	100.00%
πC22-C27	1.66105	54.41%	45.59%	0.7376($sp^{1.00}$)C22 0.6752($sp^{1.00}$)C27	0.00%	100.00%
πC23-C24	1.80466	46.97%	53.03%	0.6853($sp^{99.99}$)C23 0.7282($sp^{99.99}$)C24	0.03%	99.97%
πC28-C30	1.76351	48.85%	51.15%)	0.6989($sp^{1.00}$)C28 0.7152($sp^{1.00}$)C30	0.00%	100.00%
πC31-C39	1.64191	46.25%	53.75%	0.6801($sp^{1.00}$)C 0.7331($sp^{1.00}$)C	0.00%	100.00%
πC32-C34	1.69946	52.33%	47.67%	0.7234($sp^{1.00}$)C32 0.6904($sp^{1.00}$)C34	0.00%	100.00%
πC36-C37	1.62065	55.68%	44.32%	0.7462($sp^{1.00}$)C36 0.6657($sp^{1.00}$)C37	0.00%	100.00%
n2O1	1.73516	-	-	$sp^{99.99}$	0.11%	99.89%
n1N3	1.53064	-	-	$sp^{99.99}$	0.02%	99.98%
n2O6	1.84943	-	-	$sp^{1.00}$	0.01%	99.99%
π*N4-N5	0.48291	48.96%	51.04%	0.6997($sp^{1.00}$)N4 -0.7144($sp^{1.00}$)N5	0.02%	99.98%
π*O7-C41	0.15592	33.70%	66.30%	0.5805($sp^{1.00}$)O7 -0.8143($sp^{1.00}$)C41	0.00%	100.00%
π*C22-C27	0.37687	45.59%	54.41%	0.6752($sp^{1.00}$)C22 -0.7376($sp^{1.00}$)C27	0.00%	100.00%
π*C31-C39	0.39409	53.75%	46.25%	0.7331($sp^{1.00}$)C31 -0.6801($sp^{1.00}$)C39	0.00%	100.00%

3c-Compound						
Bond(A-B)	**ED/e**	**EDA%**	**EDB%**	**NBO**	**S%**	**P%**
πO1-C31	1.97796	67.41%	32.59%	0.8210(sp$^{1.00}$)O1 0.5709(sp$^{1.00}$)C31	0.00%	100.00%
πN4-N 5	1.89163	50.94%	49.06%	0.7138(sp$^{1.00}$) N4 0.7004(sp$^{1.00}$) N5	0.00%	100.00%
πC13 -C15	1.72141	50.60%	49.40%	0.7114(sp$^{1.00}$) C13 0.7028(sp$^{1.00}$) C15	0.00%	100.00%
πC17 -C19	1.71471	50.92%	49.08%	0.7136(sp$^{1.00}$) C17 0.7005(sp$^{1.00}$) C19	0.00%	100.00%
πC21 -C27	1.55199	48.20%	51.80%	0.6943(sp$^{1.00}$)C21 0.7197(sp$^{1.00}$)C27	0.00%	100.00%
πC22 -C24	1.77975	49.46%	50.54%	0.7033(sp$^{1.00}$) C22 0.7109(sp$^{1.00}$) C24	0.00%	100.00%
πC26 -C32	1.65911	54.71%	45.29%	0.7397(sp$^{1.00}$)C26 0.6730(sp$^{1.00}$) C32	0.00%	100.00%
πC28 -C29	1.80564	46.56%	53.44%	0.6823(sp$^{1.00}$) C28 0.7311(sp$^{1.00}$) C29	0.00%	100.00%
πC33 -C35	1.76411	48.78%	51.22%	0.6984(sp$^{1.00}$)C33 0.7157(sp$^{1.00}$)C35	0.00%	100.00%
πC36 -C44	1.63354	46.08%	53.92%	0.6788(sp$^{1.00}$) C36 0.7343(sp$^{1.00}$) C44	0.00%	100.00%
πC37 -C39	1.69556	52.62%	47.38%	0.7254(sp$^{1.00}$) C37 0.6883(sp$^{1.00}$) C39	0.00%	100.00%
πC41 -C42	1.61482	55.79%	44.21%	0.7469(sp$^{1.00}$) C41 0.6649(sp$^{1.00}$)C42	0.00%	100.00%
n2O1	1.82662	-	-	sp$^{99.99}$	0.12%	99.88%
n2O2	1.74012	-	-	sp$^{1.00}$	0.00%	100.00%
n1N3	1.53027	-	-	sp$^{99.99}$	0.02%	99.98%
n1N4	1.95583	-	-	&p$^{0.95}$	51.20%	48.80%
n1N5	1.92797	-	-	sp$^{1.51}$	39.83%	60.17%
n2O6	1.84558	-	-	sp$^{1.00}$	0.01%	99.99%
n2O47	1.89625	-	-	sp$^{1.00}$	0.01%	99.99%
π*O1-C 31	0.30201	32.59%	67.41%	0.5709(sp$^{1.00}$) O1 -0.8210(sp$^{1.00}$)C 31	0.00%	100.00%
π*C21 -C 27	0.46949	51.80%	48.20%	0.7197(sp$^{1.00}$) C21 -0.6943(sp$^{1.00}$)C 27	0.00%	100.00%
π*C26 -C 32	0.37585	45.29%	54.71%	0.6730(sp$^{1.00}$) C26 -0.7397(sp$^{1.00}$)C 32	0.00%	100.00%
π*C36 -C 44	0.39530	53.92%	46.08%	0.7343(sp$^{1.00}$) C36 -0.6788(sp$^{1.00}$)C 44	0.00%	100.00%
π*C46 -O 47	0.13208	65.72%	34.28%	0.8107(sp$^{1.00}$) C46 -0.5855(sp$^{1.00}$)O47	0.00%	100.00%

3d-Compound						
Bond(A-B)	**ED/e**	**EDA%**	**EDB%**	**NBO**	**S%**	**P%**
πO2-C26	1.97752	67.37%	32.63%	0.8208(sp$^{1.00}$)O2 0.5713 (sp$^{1.00}$)C26	0.01%	99.99%
πN4-N 5	1.89261	51.05%	48.95%	0.7145(sp$^{1.00}$) N4 0.6996(sp$^{1.00}$) N5	0.00%	100.00%
πO7-C41	1.97703	65.72%	34.28%	0.8107(sp$^{1.00}$) O7 0.5855(sp$^{1.00}$) C41	0.00%	100.00%
πC8 -C10	1.71834	50.52%	49.48%	0.7108(sp$^{1.00}$) C8 0.7034(sp$^{1.00}$) C10	0.00%	100.00%
πC12 -C17	1.55346	49.49%	50.51%	0.7035(sp$^{1.00}$) C12 0.7107(sp$^{1.00}$) C17	0.00%	100.00%
πC13 -C15	1.72614	51.33%	48.67%	0.7164(sp$^{1.00}$)13 0.6976(sp$^{1.00}$) C15	0.00%	100.00%
πC18 -C20	1.74378	48.23%	51.77%	0.6945(sp$^{1.00}$) C18 0.7195(sp$^{1.00}$) C20	0.00%	100.00%
πC22 -C27	1.66067	54.41%	45.59%	0.7376(sp$^{1.00}$) C22 0.6752(sp$^{1.00}$) C27	0.00%	100.00%
πC23 -C24	1.80491	46.98%	53.02%	0.6854(sp$^{1.00}$) C23 0.7281(sp$^{1.00}$) C24	0.00%	100.00%
πC28 -C30	1.76315	48.77%	51.23%	0.6983(sp$^{1.00}$) C28 0.7158(sp$^{1.00}$) C30	0.00%	100.00%
πC31 -C39	1.63368	46.09%	53.91%	0.6789(sp$^{1.00}$) C31 0.7342(sp$^{1.00}$) C39	0.00%	100.00%
πC32 -C34	1.69548	52.62%	47.38%	0.7254(sp$^{1.00}$) C32 0.6883(sp$^{1.00}$) C34	0.00%	100.00%
πC36 -C37	1.61478	55.78%	44.22%	0.7469(sp$^{1.00}$) C36 0.6650(sp$^{1.00}$) C37		
n2O1	1.73523	-	-	(sp$^{99.99}$)	0.02%	99.98%
n2O2	1.82840	-	-	(sp$^{99.99}$)	0.11%	99.89%
n1N3	1.52939	-	-	(sp$^{99.99}$)	0.02%	99.98%
n2O6	1.84581	-	-	(sp$^{99.99}$)	0.01%	99.99%
π*O2-C 26	0.30274	32.63%	67.37%	0.5713(sp$^{1.00}$) O2 -0.8208(sp$^{1.00}$)C 26	0.00%	100.00%
π*O7-C 41	0.13196	34.28%	65.72%	0.5855(sp$^{1.00}$) O7 -0.8107(sp$^{1.00}$)C 41	0.00%	100.00%
π*C12 -C 17	0.46366	50.51%	49.49%	0.7107(sp$^{1.00}$) C12 -0.7035(sp$^{1.00}$)C 17	0.00%	100.00%
π*C22 -C 27	0.37704	45.59%	54.41%	0.6752(sp$^{1.00}$) C22 -0.7376(sp$^{1.00}$)C 27	0.00%	100.00%
π*C31 -C 39	0.39520	53.91%	46.09%	0.7342(sp$^{1.00}$) C31 -0.6789(sp$^{1.00}$)C 39	0.00%	100.00%

IV. Conclusions

In conclusion we synthesized coumarin triazole hybrids and confirmed their structures using analytical technique like ^{1}H NMR, ^{13}CNMR, FT-IR and LC-MS. Using both experimental and computational techniques, we have understood solvatochromic behaviour, structure and charge transfer properties and other properties of **3a**, **3b**, **3c** and **3d**molecules. The DFT/B3LYP/6-311++G (d, p) basis set is utilized to obtain the optimized geometries of the studied molecules. Using a variety of solvents, solvatochromic shift techniques are used to calculate the ground and excited state dipole moments of **3a**, **3b**, **3c** and **3d**molecules. It has been noted that, the excited state dipole moment is noticeably larger than the ground state dipole moment in all the studied molecules. These results conclude that excited states are having higher polar nature than ground state dipole moments. It shows excited states are larger charge transfer nature compared to the ground states.

Conflicts of interest

There are no conflicts to declare.

Acknowledgements

We are thankful to the university scientific instrument centre (USIC) and (SAIF), Karnatak University, Dharwad for providing the spectral data.

References

[1] E. Kabir, M. Uzzaman, A Review On Biological And Medicinal Impact Of Heterocyclic Compounds, Results In Chemistry 4 (2022) 100606. Https://Doi.Org/10.1016/J.Rechem.2022.100606.

[2] H. Gao, Q. Zhang, J.M. Shreeve, Fused Heterocycle-Based Energetic Materials (2012–2019), J. Mater. Chem. A 8 (2020) 4193–4216. Https://Doi.Org/10.1039/C9ta12704f.

[3] S.S. Murphree, Chapter 2 - Heterocyclic Dyes: Preparation, Properties, And Applications, In: G. Gribble, J.A. Joule (Eds.), Progress In Heterocyclic Chemistry, Elsevier, 2011: Pp. 21–58. Https://Doi.Org/10.1016/S0959-6380(11)22002-6.

[4] G. Pfeifer, F. Chahdoura, M. Papke, M. Weber, R. Szűcs, B. Geffroy, D. Tondelier, L. Nyulászi, M. Hissler, C. Müller, Synthesis, Electronic Properties And Oled Devices Of Chromophores Based On Λ5-Phosphinines, Chemistry – A European Journal 26 (2020) 10534–10543. Https://Doi.Org/10.1002/Chem.202000932.

[5] T.V. Soumya, P. Thasnim, D. Bahulayan, Step-Economic And Cost Effective Synthesis Of Coumarin Based Blue Emitting Fluorescent Dyes, Tetrahedron Letters 55 (2014) 4643–4647. Https://Doi.Org/10.1016/J.Tetlet.2014.06.071.

[6] N. Bin Darwish, A. Kurdi, S. Alshihri, T. Tabbakh, Organic Heterocyclic-Based Colorimetric And Fluorimetric Chemosensors For The Detection Of Different Analytes: A Review (From 2015 To 2022), Materials Today Chemistry 27 (2023) 101347. Https://Doi.Org/10.1016/J.Mtchem.2022.101347.

[7] X. Wu, R. Su, Y. Zhao, H. Ma, X. Liu, L. Qian, M. Han, W. Su, T. Yu, Photo- And Electro-Luminescence Properties Of Two Coumarin-Triarylimidazole Hybrid Derivatives, New Journal Of Chemistry 46 (2022) 212–220. Https://Doi.Org/10.1039/D1nj04676d.

[8] Y. Li, Z. Yang, B. Hao, S. Wang, C. Ouyang, A. Cao, Synthesis And Nonlinear Optical Properties Of Novel Conjugated Small Molecules Based On Coumarin Donor, J Mater Sci: Mater Electron 30 (2019) 19977–19983. Https://Doi.Org/10.1007/S10854-019-02364-Z.

[9] M.S. Ebied, M. Dongol, M. Ibrahim, M. Nassary, S. Elnobi, A.A. Abuelwafa, Structural And Optical Properties Of Nanocrystalline 3-(2-Benzothiazolyl)-7-(Diethylamino) Coumarin (C6) Thin Films For Optoelectronic Application, J. Electron. Mater. 51 (2022) 5770–5782. Https://Doi.Org/10.1007/S11664-022-09792-4.

[10] S. Noreen, A. Mansha, S. Asim, Investigating The Use Of Coumarin Derivatives As Lasers, J Fluoresc (2023). Https://Doi.Org/10.1007/S10895-023-03459-X.